Large-scale Monolithic Fused-Silica Mirror Suspension for Third-Generation Gravitational-Wave Detectors

A. V. Cumming⊙,* R. Jones, G. D. Hammond, J. Hough⊙, I. W. Martin⊙, and S. Rowan

SUPA (Scottish Universities Physics Alliance), Institute for Gravitational Research, School of Physics and Astronomy, University of Glasgow, Glasgow G12 8QQ, United Kingdom

Thermal noise from the suspension fibers used in the mirror pendulums in current gravitational-wave detectors is a critical noise source. Future detectors will require improved suspension performance with the specific ability to suspend much heavier masses to reduce radiation pressure noise, while retaining good thermal noise performance. In this paper we propose and experimentally demonstrate a design for a large-scale fused-silica suspension, demonstrating its suitability for holding an increased mass of 160 kg. We demonstrate the concepts for improving thermal noise via longer suspension fibers supporting a higher static stress. We present a full thermal noise analysis of our prototype, meeting requirements for conceptual third-generation detector designs such as the high frequency interferometer of the Einstein Telescope, and closely approaching that required for Cosmic Explorer.

I. INTRODUCTION

Advanced second-generation interferometric gravitational-wave observatories, including Advanced LIGO (aLIGO) [1] and Advanced Virgo (AdV) [2], have regularly acquired signals from astronomical events following on from aLIGO's initial binary black hole inspiral detection in 2015 [3]. To date, over 40 confirmed black hole mergers have been recorded [4], including one resulting in an intermediate-mass black hole [5], and two neutron star inspirals [6,7]. Most recently, two black hole-neutron star inspirals were observed [8], providing further scientific insight.

Mirrors in the interferometer's arms have final-stage suspensions constructed from fused-silica mirrors, each hanging from four precisely manufactured silica fibers. This is key in providing appropriate levels of noise at low frequencies (10–30 Hz), as it allows the optimization and minimization of thermal displacement noise [9], $x(\omega)$, given by [10,11]

$$x(\omega) = \sqrt{\frac{4k_B T}{m\omega}\left(\frac{\omega_o^2 \phi(\omega)}{\omega_o^4 \phi^2(\omega) + (\omega_o^2 - \omega^2)^2}\right)}, \quad (1)$$

where T is the temperature, m is the pendulum mass, $\phi(\omega)$ is the mechanical loss of the pendulum mode, of resonant angular frequency ω_o, k_B is Boltzmann's constant, and ω is the angular frequency of interest. Choosing ultra low mechanical loss fused silica for the suspension fibers

therefore permits a significant reduction in the suspension thermal noise [12–15].

Future detectors will require a radical upscaling of the suspended mass, from the current 40 kg to 160 kg or even larger. This is driven by a need to reduce radiation pressure noise [16]. Also, the optic's larger-diameter front surface allows larger beam size, reducing coating thermal noise [17]. However, this mass upscale must also not detrimentally affect suspension thermal noise performance. Therefore, suspension design must be carefully considered, and demonstrated experimentally. In this paper we propose a set of design principles for next-generation silica suspensions, highlighting their possibilities and limitations in terms of noise performance and internal mode frequencies. Employing these principles, we have forged toward larger suspensions by exhibiting a successful long-term experimental prototype suspension, hanging 160 kg on detector-quality fibers, laser-welded to silica attachment cones. Projected thermal noise performance is analyzed using finite-element analysis (FEA) models. When scaled to the proposed mirror masses, performance is seen to be more than sufficient to meet that required for currently proposed conceptual detector designs.

Currently, final-stage suspension designs of aLIGO and AdV have mirrors suspended from four "dumbbell"-shaped silica fibers [18], with the fiber shape precisely controlled [19] to minimize thermoelastic noise [20], which results from temperature fluctuations in the fiber [21,22]. Recent studies [23] on currently installed aLIGO suspensions have demonstrated extremely low mechanical loss, actually yielding better performance than previously anticipated. There are two distinct, but

---

*alan.cumming@glasgow.ac.uk

potentially complementary, paths that final-stage suspension systems may take for future third-generation telescopes. The first is to reduce thermal noise directly, via cryogenic cooling of the mirrors and suspensions. This is an extreme technical challenge requiring changing material from silica to silicon or sapphire [24]. The second path is further upgrading silica suspensions, as will be discussed in this paper. For example, the future Einstein Telescope (ET) proposes using enhanced room-temperature silica suspensions in its high-frequency interferometer (ET-HF), with the instrument envisaging use of heavier silica suspensions up to 200 kg to broaden the available frequency band to higher levels, in excess of 10 Hz [25,26]. Improved sensitivity at frequencies below 30 Hz comes from a cryogenic instrument with silicon suspensions and optics (ET-LF) proposed for parallel operation with ET-HF.

Interestingly, Cosmic Explorer (CE) envisages use of very large room-temperature suspensions of up to 320 kg, possibly achieving similar sensitivity to ET using longer interferometer arms, without cryogenics [27,28].

Here, we propose three core concepts for improvement of final-stage fused-silica suspension performance.

II. CONCEPT ONE - INCREASED MASS OF THE SUSPENDED CAVITY MIRRORS

A strong driver for increasing the mirror mass is reduction of radiation pressure noise, which is inversely proportional to the mass [16]. In addition, Eq. (1) shows that the displacement thermal noise of a mirror is also proportional to $m^{-1/2}$. Thus, by simply increasing the mirror's mass, the thermal noise performance can be improved. Typically,
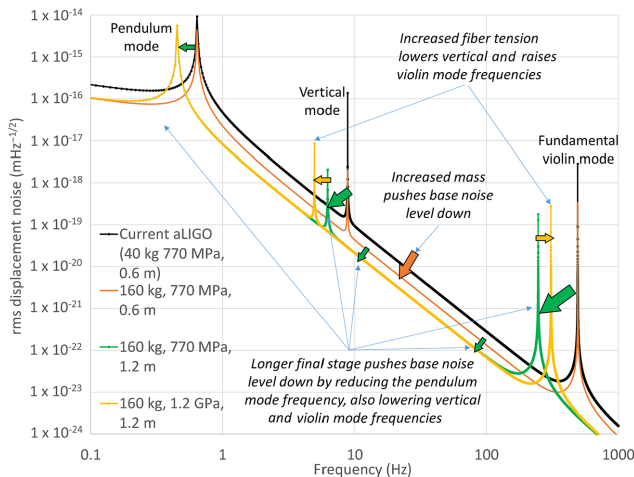

FIG. 1. Theoretical calculation of suspension thermal displacement noise of a single mirror suspension, showing the sequence of steps taken to improve performance, by (a) increasing the mass, (b) increasing the final-stage length, (c) increasing the fiber's suspended stress.

a mass gain of a factor of 4–8 over the current 40 kg is envisaged for future suspensions [25], For a factor of 4, this reduces noise by a factor 2, as shown in the red curve in Fig. 1, where fiber cross section has been scaled to maintain fiber stress.

III. CONCEPT TWO - INCREASED FINAL-STAGE LENGTH

The second concept is to lengthen the final stage's suspension fibers. By doubling their length to 120 cm, the pendulum mode is pushed down in frequency by a factor of $\sqrt{2}$. This frequency reduction effectively moves the whole curve to the left, which results in an additional thermal noise gain, yielding the green curve in Fig. 1.

This length increase also provides the benefit of reducing the vertical bounce mode frequency by factor of $\sqrt{2}$ from 8.8 to 5 Hz, opening up a greater range of frequencies in the sub-10 Hz band. One disadvantage of this change is the resulting decrease in frequency of the violin modes, which encroach further into the detection band. Our third strategy change aims to help minimize this.

IV. CONCEPT THREE - INCREASED FINAL-STAGE SILICA FIBER STRESS

Due to the violin mode frequency's direct dependence on length, the fundamental mode's frequency halves to ~246 Hz when fiber length is doubled. However, fiber diameter consistency improvements [29] allow a final strategy of reduction in the diameter of the fiber's central section, increasing the suspended stress in this region of the fiber. aLIGO has a static fiber stress of 770 MPa, but fibers have been demonstrated as having ultimate tensile strengths of up to 3–4 GPa [27]. As such, increasing the stress to 1.2–1.5 GPa is a credible suspension stress for long-term use, which pushes the violin modes back up in frequency to above 300 Hz as shown by the yellow curve in Fig. 1. While the original mode frequency of approximately 500 Hz cannot be fully recovered, this is a necessary compromise, with the added benefit of reducing the vertical frequency by an additional factor of $\sqrt{2}$.

We have successfully built a prototype suspension employing these principles. A number of practical design factors must also be considered, including fiber shapes and silica attachment piece ("ear") design, for ease of laser welding.

V. FIBER SHAPE

The fiber design aims to follow on in concept from those used in aLIGO and AdV, via nulling thermoelastic noise that results from temperature fluctuations along the fiber, that translate into motion via the material's thermal expansion coefficient [20]. Thermoelastic loss, ϕ_{thermo}, is

given by

$$\phi_{\text{thermo}}(\omega) = \frac{YT}{\rho C}\left(\alpha - \sigma_o \frac{\beta}{Y}\right)^2 \left(\frac{\omega\tau}{1 + (\omega\tau)^2}\right), \qquad (2)$$

with

$$\tau = \frac{1}{4.32\pi}\frac{\rho C d^2}{\kappa}, \qquad (3)$$

where Y is the fiber's Young's modulus, C is specific heat capacity per unit mass, κ is thermal conductivity, ρ is density, α is the linear thermal expansion coefficient, σ_o is the fiber's loaded static stress, $\beta = (1/Y)(dY/dT)$ is the thermal elastic coefficient, and d is the fiber diameter. Nulling occurs when $\alpha - \sigma_o(\beta/Y) = 0$, giving diameter

$$d_{\text{null}} = 2r_{\text{null}} = 2\sqrt{\frac{F\beta}{\pi\alpha Y}}, \qquad (4)$$

where F is the vertical tension on a single fiber occurring due to the suspended mass. This yields $d_{\text{null}} = 1644\ \mu$m, for 160 kg mass held on four fibers. A length of 30 mm at the fiber ends was chosen to be this diameter for the nulling region, to ensure as much elastic bending energy is stored in a nulled area, with a minimal amount contained in the starting ("stock") material at the fiber's ends used for welding to the ears [30]. Fibers for aLIGO were pulled from 3 mm diameter fused-silica rod, leaving approximately 10 mm of this material at the fiber ends. This provided enough material to hold the fiber securely while welding occurred, while minimizing the amount of elastic bending energy occurring in this region. It is important to keep the proportion of elastic energy in the weld region to an acceptable level (typically below 10% in aLIGO), due to it having higher loss than the surrounding material [23].

In order to understand which areas of the fiber contribute to the dissipation, we need to consider where the elastic bending energy resides in the fiber [31]. If the mass is increased on a 3 mm stock fiber, significantly more elastic energy is pushed into the stock region of the fiber and out of the thermoelastic nulling region, as is shown in Fig. 2. The solution to maintain a low elastic energy content in the stock material is to increase its diameter from 3 to 5 mm. Figure 2 shows an ANSYS FEA case study of the energy distribution at the fiber end for three different cases:

  (i)   An aLIGO fiber with end diameter of 3 mm, holding 10 kg (for total mass 40 kg)
  (ii)   The same fiber holding 40 kg (for total mass 160 kg)
  (iii)   A fiber with increased end diameter of 5 mm holding 40 kg.

Increasing the fiber end diameter to 5 mm gives a smaller level of elastic energy in the stock material than
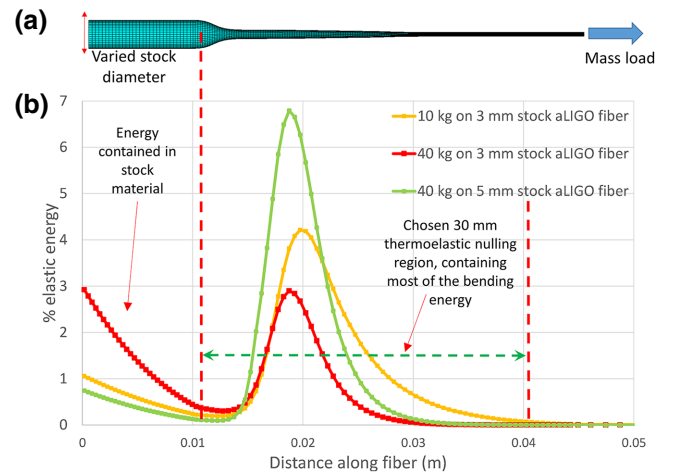

FIG. 2. (a) FEA model of an aLIGO fiber, with its shorter approximately 20 mm nulling region. (b) Elastic energy distribution at equivalent position along the fiber, showing results from different suspended masses and different stock material diameters, together with the proposed thermoelastic nulling region.

for an equivalent 3 mm fiber. It also results in a lower proportion (16%) of energy in the stock compared to the original aLIGO situation (25%), this being an additional improvement. The remaining 84% of the bending energy is contained in the 30 mm nulling region, as shown in Fig. 2.

The central fiber section in aLIGO is thinned to achieve optimal violin and vertical mode frequencies. For large-scale suspensions, this technique will also be employed. For a 160 kg suspension, to achieve a working stress of 1.2 GPa, a fiber of diameter 646 μm is required.
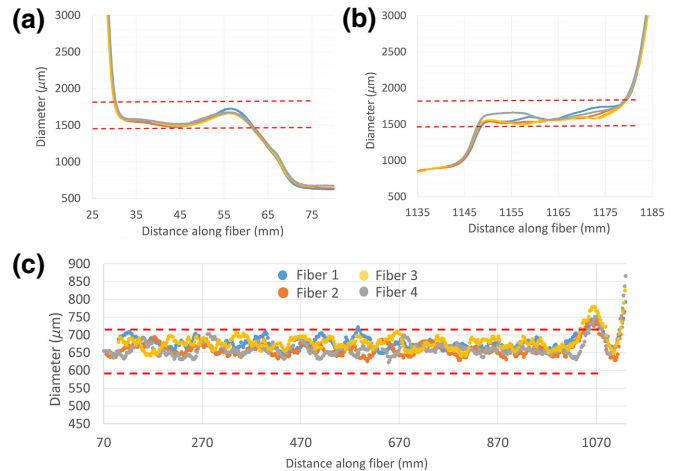

FIG. 3. (a) Diameter profile of bottom thermoelastic loss nulling region of fibers used in the prototype suspension. (b) Top thermoelastic loss nulling region profile. (c) Central region profile. Red dashed lines show a guide to the eye of ±10% from the nominal required dimensions.

Fibers were pulled from 5 mm diameter Suprasil-3 stock material which was laser-polished prior to pulling to maximize strength [32]. All fibers were pulled on a lengthened version of the laser pulling machine detailed in Ref. [19], and were carefully profiled after pulling and welding on a similarly uprated dimensional characterization machine [33] as shown in Figs. 3(a) and 3(b), with fibers' dimensions lying well within 10% of the required dimensions. The maximum fiber stress at any individual point was 1.29 GPa, and the average stress in the fiber's central section was 1.12 GPa. Their average diameter was 670 μm, approximately 4% above the nominal 646 μm diameter. Future loading tests may hang up to 200 kg, with the absolute maximum stress in this case being envisaged to be a reasonable 1.60 GPa.

VI. LASER WELDING

Attachment of the fibers uses the same principle of 10.6 μm wavelength CO_2 laser welding that was successfully used in aLIGO. However, for thicker stock material, testing has shown that the nominal 120 W laser power available was insufficient. Therefore, a laser with increased power of up to 450 W was used. Welding was undertaken using a conical mirror arrangement of the fiber pulling machine [19], allowing uniform heating from all sides of the fiber and ear tip ("horn"). Additional visibility was supplied using multiple 14-bit cameras [29]. This improved procedure has resulted in extremely good-quality consistent welds, achievable more quickly. Research is ongoing towards a miniature portable version of this optical system for use at detector sites, to allow more amenable welding of suspensions on site at the ends of the interferometer arms.

The horn of the projected ear has been simplified from the rectangular horn with curved edges used in aLIGO, to a circular cone tip with 45° angle. This eases welding further by keeping both surface geometries circular at the interface point. The sharpness of the cone angle helps keep elastic energy out of the ear and deeper weld region, maintaining as much of it in the fiber as possible. The horns were clamped to bespoke metal clamps for this test, however it is ultimately envisaged that that a conical horn would be incorporated into an upscaled aLIGO style ear [30], research on which is ongoing.

The completed welded four-fiber prototype suspension is shown in Fig. 4.

Fiber profiles and welding were initially tested on two single-fiber 40 kg suspensions, prior to the four-fiber full hang, with the single-fiber tests successfully lasting multiple months prior to the full suspension build. The four-fiber prototype suspension has been hanging in a standard laboratory setting in air for more than 3 years since 2018, accumulating just over 100 000 cumulative fiber hanging hours to date.
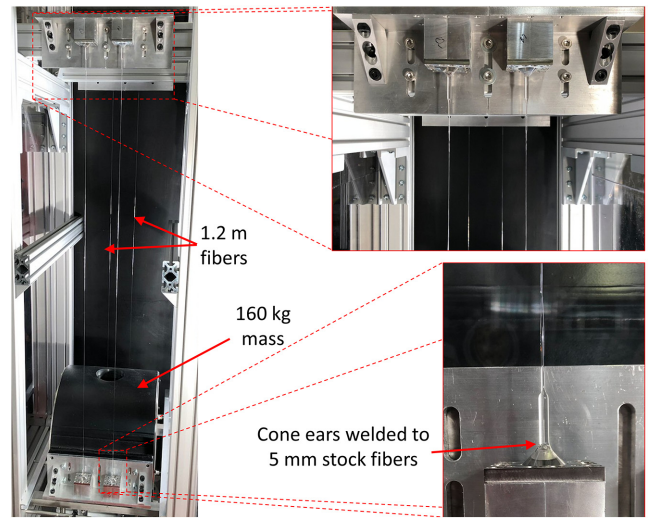

FIG. 4. Completed monolithic conceptual prototype using 160 kg mass and four fibers, 1.2 m in length, supporting approximately 1.2 GPa stress. Insets show 5 mm stock at ends of fibers welded to cone attachment ears and clamped to mass sides.

VII. PROJECTED PERFORMANCE

The profile data for Figure 3 were directly imported into ANSYS to construct an accurate FEA model of the suspension using techniques described in Refs. [30,31], here also including accurate weld geometries. The FEA model was used to evaluate the elastic energy distribution for each of the suspension's resonant modes to weight the mechanical loss contribution of each loss mechanism as previously outlined in Ref. [30].

The first mechanism is residual thermoelastic loss in sections of the fiber outside the nulling region described by Eq. (2). Secondly, surface loss in the ith element of the fiber model is given by [21]

$$\phi_{\text{surface}} = \frac{8h\phi_s}{d_i}, \tag{5}$$

where $h\phi_s$ is the product of the mechanical loss of the material surface, ϕ_s, and the depth, h, over which surface loss mechanisms are believed to occur, and d_i is the average diameter of the ith element along the fiber length. Using the analyses recently undertaken by the authors, $h\phi_s$ was taken to be 2.5×10^{-12} m [23].

The third mechanism is weld loss, the excess loss associated with the welded attachment regions at the fiber ends. The value taken was 1.4×10^{-7}, again from the authors' recent analyses [23], with the observed weld region being 2 mm in length at the fiber ends [30], typically containing less than 5% of the elastic energy in this suspension.

Finally, bulk loss is the internal friction of the fiber material given by

$$\phi_{\text{bulk}}(\omega) = C_2 \left(\frac{\omega}{2\pi} \right)^{0.77}, \qquad (6)$$

where C_2 is an empirically evaluated constant [13]. For the fiber material, Suprasil-3, $C_2 = 1.18 \pm 0.04 \times 10^{-11}$.

The total mechanical loss is the sum of these effects, was evaluated as previously [23], using

$$\phi_{\text{resonance } j}(\omega) = \frac{E_{\text{total } j}}{E_{\text{gravity}}} \left(\sum_{i=1}^{n} \frac{E_i}{E_{\text{total } j}} (\phi_{\text{thermo}}(\omega) + \phi_{\text{surface}} \right.$$
$$\left. + \phi_{\text{bulk}}(\omega)) + \frac{E_{\text{welds}}}{E_{\text{total } j}} \phi_{\text{welds}} \right), \qquad (7)$$

where, E_i is the energy stored in the ith FEA model element, E_{welds} is the energy in the weld region, and $E_{\text{total } j}$ is jth mode's total elastic energy. $E_{\text{total } j}/E_{\text{gravity}}$ is the jth mode's "dissipation dilution," a reduction factor occurring because a significant proportion of the pendulum's potential energy is stored in the lossless gravitational field, and is evaluated from FEA [31].

The thermal horizontal displacement noise was then evaluated from Eq. (1). Vertical noise was calculated via Eq. (17) in Ref. [30], and the violin-mode thermal noise [34] was determined via Eq. (18) in Ref. [30]. The resulting thermal noise displacement curve is shown in Fig. 5.

ET-HF will eventually operate in combination with ET-LF, with the latter dominant below 30 Hz. However, with the technological challenge of ET-LF's cryogenics [35], it is plausible that there may be operational periods, particularly in ET's early days, when ET-HF could be running solo. ET-HF will be dominated strongly by suspension thermal noise between 7 and 30 Hz, this being some six times higher than the next contributing noise source, radiation pressure noise. At 10 Hz, the design requires a total noise of 9.90×10^{-20} mHz$^{-1/2}$; this being dominated primarily by suspension thermal noise, and our proposed suspension provides a considerably lower value of 2.85×10^{-20} mHz$^{-1/2}$. Thus, deployment of the proposed suspension would yield an immediate gain of a factor $3.5\times$ in detector sensitivity. This room temperature gain with proven technology could enhance any early rollout of third-generation room-temperature instruments, increasing astronomical reach between 7 and 30 Hz. The reduced suspension thermal noise is also less than a factor 2 above radiation pressure noise, and further gains may be achievable to make suspension noise no longer dominant using a test mass of 200 kg or higher, for example.

Cosmic Explorer's room temperature curve is an example of this, with anticipated use of 320 kg silica payloads, and fibers of length 2 m [28]. By using a simple scaling of our 160 kg, 1.2 m suspension, a mass of 320 kg would give a factor of $\sqrt{2}$ improvement, and a 2 m suspension a factor of $\sqrt{1.7}$ improvement, meaning a cumulative factor of $\sqrt{3.4} = 1.8$. Simple scaling of our prototype shows that it approaches what would be required for CE. At 10 Hz for example, CE requires 1.33×10^{-20} mHz$^{-1/2}$, and our suspension, simply scaled, approaches this with value approximately 1.58×10^{-20} mHz$^{-1/2}$. Further gain with use of even thicker stock material of up to 6 or 7 mm for higher masses is anticipated. Thus, with the groundwork laid with the prototype suspension demonstrated in this paper, future research will focus on practical demonstration of a 320 kg CE-capable payload, and this research is ongoing.

VIII. CONCLUSIONS

We have proposed three distinct concepts for radically upscaling final-stage fused-silica quasi-monolithic suspensions for gravitational-wave detectors, including increasing the test mass size, increasing suspension length, and increasing stress in the fibers. We have demonstrated production of suitable fibers, and welds suitable for future detector use, and have constructed a large-scale long-term quadruple-fiber suspension, which has been successfully hanging for over 3 years. Projected noise performance, using FEA, has shown significantly lower suspension thermal noise than previous conceptual designs such as ET-HF, providing a potential factor of 3.5 improvement between 7 and 30 Hz, and lays the groundwork for future upscaling to 320 kg for CE.
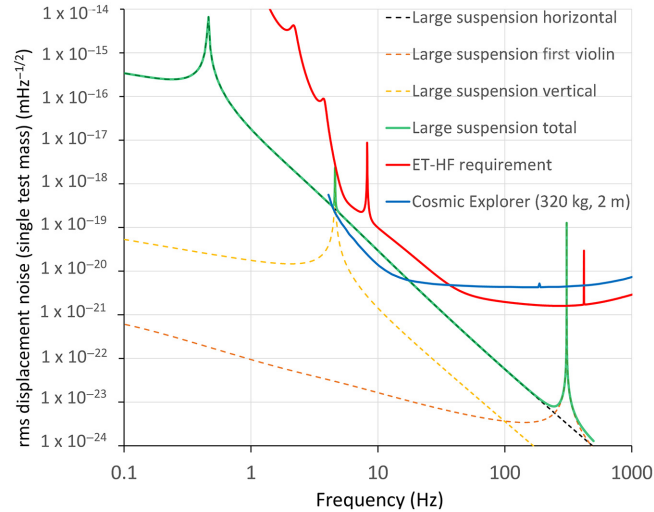

FIG. 5. Displacement thermal noise spectrum of large suspension prototype, compared to the ET-HF design requirement [35], and the CE room-temperature design. CE has heavier masses of 320 kg and 2 m suspension fibers 2 m in length here [28].

---

[1] J. Aasi, B. P. Abbott, R. Abbott, T. Abbott, M. R. Abernathy, K. Ackley, C. Adams, T. Adams, P. Addesso, R. X. Adhikari, *et al.*, Advanced LIGO, Class. Quantum Gravity **32**, 074001 (2015).

[2] F. Acernese, M. Agathos, K. Agatsuma, D. Aisa, N. Allemandou, A. Allocca, J. Amarni, P. Astone, G. Balestri, G. Ballardin, *et al.*, Advanced Virgo: A second-generation interferometric gravitational wave detector, Class. Quantum Gravity **32**, 024001 (2014).

[3] B. P. Abbott, R. Abbott, T. D. Abbott, M. R. Abernathy, F. Acernese, K. Ackley, C. Adams, T. Adams, P. Addesso, R. X. Adhikari, *et al.*, Observation of Gravitational Waves From a Binary Black Hole Merger, Phys. Rev. Lett. **116**, 061102 (2016).

[4] R. Abbott, T. D. Abbott, S. Abraham, F. Acernese, K. Ackley, A. Adams, C. Adams, R. X. Adhikari, V. B. Adya, C. Affeldt, *et al.*, GWTC-2: Compact Binary Coalescences Observed by LIGO and Virgo during the First Half of the Third Observing Run, Phys. Rev. X **11**, 021053 (2021).

[5] R. Abbott, T. D. Abbott, S. Abraham, F. Acernese, K. Ackley, C. Adams, R. X. Adhikari, V. B. Adya, C. Affeldt, M. Agathos, *et al.*, GW190521: A Binary Black Hole Merger with a Total Mass of 150 $M_\odot$, Phys. Rev. Lett. **125**, 101102 (2020).

[6] B. P. Abbott, R. Abbott, T. D. Abbott, F. Acernese, K. Ackley, C. Adams, T. Adams, P. Addesso, R. X. Adhikari1, V. B. Adya, *et al.*, GW170817: Observation of Gravitational Waves From a Binary Neutron Star Inspiral, Phys. Rev. Lett. **119**, 161101 (2017).

[7] B. P. Abbott, R. Abbott, T. D. Abbott, S. Abraham, F. Acernese, K. Ackley, C. Adams, R. X. Adhikari, V. B. Adya, C. Affeldt, *et al.*, GW190425: Observation of a compact binary coalescence with total mass ∼3.4 $M_\odot$, Astrophys. J. Lett. **892**, L3 (2020).

[8] R. Abbott, T. D. Abbott, S. Abraham, F. Acernese, K. Ackley, A. Adams, C. Adams, R. X. Adhikari, V. B. Adya, C. Affeldt, *et al.*, Observation of gravitational waves from Two neutron star–black hole coalescences, Astrophys. J. Lett. **915**, L5 (2021).

[9] P. R. Saulson, Thermal noise in mechanical experiments, Phys. Rev. D **42**, 2437 (1990).

[10] H. B. Callen and T. A. Welton, Irreversibility and generalised noise, Phys. Rev. **83**, 34 (1951).

[11] H. B. Callen and R. F. Greene, On a theorem of irreversible thermodynamics, Phys. Rev. **86**, 702 (1952).

[12] S. Rowan and J. Hough, Gravitational wave detection by interferometry (ground and space), Living Rev. Relativ. **3**, 3 (2000).

[13] V. B. Braginsky, V. P. Mitrofanov, and K. V. Tokmakov, On the thermal noise from the violin modes of the test mass suspension in gravitational wave antennae, Phys. Lett. A **186**, 18 (1994).

[14] V. B. Braginsky, V. P. Mitrofanov, and K. V. Tokmakov, Energy dissipation in the pendulum mode of the test mass suspension of a gravitational wave antenna, Phys. Lett. A **218**, 164 (1996).

[15] S. D. Penn, G. M. Harry, A. M. Gretarsson, S. E. Kittelberger, P. R. Saulson, J. J. Schiller, J. R. Smith, S. O. Swords, *et al.*, High quality factor measured in fused silica, Rev. Sci. Instrum. **72**, 3670 (2001).

[16] S. Sakata, V. Leonhardt, S. Kawamura, K. Numata, O. Miyakawa, S. Sato, A. Nishizawa, T. Yamazaki, M. Fukushima, A. Furusawa, *et al.*, A study for reduction of radiation pressure noise in gravitational wave detectors, J. Phys.: Conf. Ser. **122**, 012020 (2008).

[17] G. M. Harry, A. M. Gretarsson, P. R. Saulson, S. E. Kittelberger, S. D. Penn, W. J. Startin, S. Rowan, M. M. Fejer, D. R. M. Crooks, G. Cagnoli, *et al.*, Thermal noise in interferometric gravitational wave detectors due to dielectric optical coatings, Class. Quantum Gravity **19**, 897 (2002).

[18] P. Willems, Dumbbell-shaped fibers for gravitational wave detectors, Phys. Lett. A **300**, 162 (2002).

[19] A. Heptonstall, M. A. Barton, A. Bell, G. Cagnoli, C. A. Cantley, D. R. M. Crooks, A. Cumming, A. Grant, G. D. Hammond, G. M. Harry, *et al.*, CO_2 laser production of fused silica fibers for use in interferometric gravitational wavedetector mirror suspensions, Rev. Sci. Instrum. **82**, 011301 (2011).

[20] G. Cagnoli and P. Willems, Effects of nonlinear thermoelastic damping in highly stressed fibers, Phys. Rev. B **65**, 174111 (2002).

[21] A. Gretarsson and G. M. Harry, Dissipation of mechanical energy in fused silica fibers, Rev. Sci. Instrum. **70**, 4081 (1999).

[22] C. J. Bell, S. Reid, J. Faller, G. D. Hammond, J. Hough, I. W. Martin, S. Rowan, and K. V. Tokmakov, Experimental results for nulling the effective thermal expansion coefficient of fused silica fibers under a static stress, Class. Quantum Gravity **31**, 065010 (2014).

[23] A. V. Cumming, B. Sorazu, E. Daw, G. D. Hammond, J. Hough, R. Jones, I. W. Martin, S. Rowan, K. A. Strain, and D. Williams, Lowest observed surface and weld losses in fused silica fibers for gravitational wave detectors, Class. Quantum Gravity **37**, 195019 (2020).

[24] S. Miyoki, in *Proc. SPIE, Ground-Based and Airborne Telescopes VIII*, 11445, 114450Z (13 December 2020). doi:10.1117/12.2560824

[25] Science Case for the Einstein Telescope https://arxiv.org/abs/1912.02622

[26] Einstein gravitational wave Telescope Conceptual Design Study (2011) https://tds.virgo-gw.eu/?call_file=ET-0106C-10.pdf

[27] B. P. Abbott, R. Abbott, T. D. Abbott, M. R. Abernathy, K. Ackley, C. Adams, P. Addesso, R. X. Adhikari, V. B. Adya, C. Affeldt, *et al.*, Exploring the sensitivity of next generation gravitational wave detectors, Class. Quantum Gravity **34**, 044001 (2017).

[28] A Horizon Study for Cosmic Explorer Science, Observatories, and Community LIGO Public Document P2100003.

[29] K. Lee, G. Hammond, J. Hough, R. Jones, S. Rowan, and A. Cumming, Improved fused silica fibers for the advanced LIGO monolithic suspensions, Class. Quantum Gravity **36,** 185018 (2019).

[30] A. V. Cumming, A. S. Bell, L. Barsotti, M. A. Barton, G. Cagnoli, D. Cook, L. Cunningham, M. Evans, G. D. Hammond, G. M. Harry, *et al.*, Design and development of the advanced LIGO monolithic fused silica suspension, Class. Quantum Gravity **29,** 035003 (2012).

[31] A. Cumming, A. Heptonstall, R. Kumar, W. Cunningham, C. Torrie, M. Barton, K. A. Strain, J. Hough, and S. Rowan, Finite element modelling of the mechanical loss of silica suspension fibers for advancedgravitational wave detectors, Class. Quantum Gravity **26,** 215012 (2009).

[32] A. Heptonstall, M. A. Barton, A. S. Bell, A. Bohn, G. Cagnoli, A. Cumming, A. Grant, E. Gustafson, G. D. Hammond, J. Hough, *et al.*, Enhanced characteristics of fused silica fibers using laser polishing, Class. Quantum Gravity **31,** 105006 (2014).

[33] A. Cumming, R. Jones, M. Barton, G. Cagnoli C, A. Cantley, D. R. M. Crooks, G. D. Hammond, A. Heptonstall, J. Hough, S. Rowan, *et al.*, Apparatus for dimensional characterization of fused silica fibers for the suspensions ofadvanced gravitational wave detectors, Rev. Sci. Instrum. **82,** 044502 (2011).

[34] C. Brif, Notes on anelastic effects and thermal noise in suspensions of test masses in interferometric gravitational-wave detectors LIGO Document T990041 (1999).

[35] Design Report update 2020 for Einstein Telescope https://apps.et-gw.eu/tds/?content=3&r=17245